The Astrophysical Journal, 881:92 (4pp), 2019 August 20 https://doi.org/10.3847/1538-4357/ab2dff

Observation of He-like Satellite Lines of the H-like Potassium K XIX Emission

M. E. Weller[1], P. Beiersdorfer[1], T. E. Lockard[1], G. V. Brown[1], A. McKelvey[1,2], J. Nilsen[1], R. Shepherd[1], V. A. Soukhanovskii[1], M. P. Hill[3], L. M. R. Hobbs[3], D. Burridge[3], D. J. Hoarty[3], J. Morton[3], L. Wilson[3], S. J. Rose[4], and P. Hatfield[5]
[1] Lawrence Livermore National Laboratory, Livermore, CA 94550, USA
[2] University of Michigan, Ann Arbor, MI 48109, USA
[3] Directorate of Research and Applied Science, AWE plc, Reading RG7 4PR, UK
[4] Plasma Physics Group, Blackett Laboratory, Imperial College London, London, SW7 2AZ, UK
[5] Clarendon Laboratory, Parks Road, Oxford, OX1 3PU, UK
Received 2018 November 27; revised 2019 June 21; accepted 2019 July 1; published 2019 August 16

Abstract

We present measurements of the H-like potassium (K XIX) X-ray spectrum and its He-like (K XVIII) satellite lines, which are situated in the wavelength region between 3.34 and 3.39 Å, which has been of interest for the detection of dark matter. The measurements were taken with a high-resolution X-ray spectrometer from targets irradiated by a long-pulse (2 ns) beam from the Orion laser facility. We obtain experimental wavelength values of dielectronic recombination satellite lines and show that the ratio of the Lyα lines and their dielectronic satellite lines can be used to estimate the electron temperature, which in our case was about 1.5 ± 0.3 keV.

Key words: atomic data – dark matter – methods: laboratory: atomic – plasmas – techniques: spectroscopic – X-rays: galaxies: clusters

1. Introduction

There has been a recent debate about the origin of a 3.5 keV X-ray emission feature measured in the Galactic Center and the Perseus galaxy cluster. The line was first detected by Bulbul et al. (2014), and it was hypothesized that the line was either caused by the decay of sterile neutrino dark matter or by an atomic transition, the intensity of which was underestimated. To offer potential solutions to the phenomenon, Jeltema & Profumo (2015) and Carlson et al. (2015) concluded that a likely candidate for the line is a pair of K XVIII lines at 3.48 and 3.52 keV and the feature is not caused by the decay of sterile neutrino dark matter. Recent observations of the Perseus galaxy cluster with the *Hitomi* satellite (Aharonian et al. 2017) have ruled out anomalously bright K XVIII lines as the cause of the 3.5 keV emission reported by Bulbul et al. (2014). However, the *Hitomi* observations appeared to identify (weak) flux from both K XVIII and K XIX. This debate and the potential presence of potassium emission lines have sparked interest in producing and verifying the associated atomic data and in studying potassium emission from laboratory sources, especially as few experiments have focused on the X-ray emission of this element and as a deeper understanding of X-ray lines generated in this region is needed (Gu et al. 2015; Shah et al. 2016).

To our knowledge, only K XVIII X-ray lines have been previously studied in the laboratory, i.e., the He-like potassium lines $1snp\ ^1P_1 \rightarrow 1s^2\ ^1S_0$ were measured in laser-produced plasmas (Feldman et al. 1974) with $n = 2$ and subsequently in a tokamak plasma from the Princeton Large Torus (PLT; Beiersdorfer et al. 1989) with $n = 2, 3$. No laboratory X-ray spectra have been reported for K XIX. Here we present a measurement of the $2p\ ^2P_{3/2} \rightarrow 1s\ ^2S_{1/2}$ Lyα_1 and $2p\ ^2P_{1/2} \rightarrow 1s\ ^2S_{1/2}$ Lyα_2 lines and the associated He-like satellite lines. The He-like satellite lines are of particular interest, because they are produced by dielectronic recombination. Such lines have been measured previously only for neighboring elements, e.g., argon (Bartiromo et al. 1985; Rice et al. 2011), calcium (Rice et al. 2014), chromium (Bartiromo et al. 1989), and iron (Decaux et al. 1991).

The paper is organized as follows. In Section 2 we present our theoretical predictions for the He-like satellite lines associated with the K XIX spectrum that were generated using the Flexible Atomic Code (FAC, Gu 2008). We also include a theoretical estimate of the relative dielectronic satellite intensity as a function of electron temperature, which was generated with the Spectroscopic Collisional-Radiative Atomic Model (SCRAM; Hansen et al. 2007; 2011). In Section 3 we present our experimental results and give wavelength estimates for two resolved dielectronic recombination lines. Section 4 concludes our study.

2. Theoretical Predictions of He-like Satellite Dielectronic Recombination Lines

A non-local thermodynamic equilibrium (non-LTE) kinetic model of potassium was developed to help in the analysis. The atomic rates were generated using FAC (version 1.1.1), which calculates energy levels, collisional excitation, collisional ionization, radiative decay, Auger decay, photoionization, and radiative recombination. The description of the energy levels for H- and He-like ions calculated using FAC are as follows: the singly excited states are included up to $n = 6$ for H-like ions, where there are a total of 30 levels, and $n = 5$ for He-ions, where there are a total of 90 levels. The doubly excited states include up to $n = 3$ for He-like ions.

Table 1 gives a list of the FAC-calculated wavelengths of the H-like and He-like potassium lines compared with previous Vainshtein & Safronova (1978), Johnson & Soff (1985), and Garcia & Mack (1965) calculations. The two H-like lines are the doublet Ly$\alpha_{1,2}$ $2p\ ^2P_{3/2,1/2} \rightarrow 1s\ ^2S_{1/2}$ resonance lines at approximately 3.3466 Å and 3.3521 Å, respectively. These FAC-calculated wavelengths are approximately 0.001 Å greater than those calculated by Vainshtein & Safronova (1978) and in agreement (to 0.0001 Å) with those calculated by Johnson & Soff (1985) and Garcia & Mack (1965). The rest of the He-like lines are on average 0.0005 Å different, with the clear majority of FAC wavelengths being slightly greater than those of the Vainshtein & Safronova (1978) calculations. The two prominent

Table 1
Theoretical Wavelengths for Potassium He-like Dielectronic Lines and H-like Resonance Lines from the Flexible Atomic Code Compared to Those from the Calculations of Vainshtein & Safronova (1978), Johnson & Soff (1985), and Garcia & Mack (1965)

Ion	Transition	FAC λ (Å)	Vainshtein/Safronova λ (Å)	Johnson/Soff λ (Å)	Garcia/Mack λ (Å)
He	$2p^2\ ^1S_0 \rightarrow 1s2p\ ^3P_1$	3.3391	3.3392	⋯	⋯
H	$2p\ ^2P_{3/2} \rightarrow 1s\ ^2S_{1/2}$	3.3466	3.3456	3.3467	3.3467
He	$2s2p\ ^1P_1 \rightarrow 1s2s\ ^3S_1$	3.3461	3.3469	⋯	⋯
H	$2p\ ^2P_{1/2} \rightarrow 1s\ ^2S_{1/2}$	3.3521	3.3510	3.3521	3.3521
He	$2p^2\ ^1S_0 \rightarrow 1s2p\ ^1P_1$	3.3552	3.3549	⋯	⋯
He	$2p^2\ ^1D_2 \rightarrow 1s2p\ ^3P_1$	3.3648	3.3646	⋯	⋯
He-T	$2s2p\ ^1P_1 \rightarrow 1s2s\ ^1S_0$	3.3664	3.3667	⋯	⋯
He	$2p^2\ ^1D_2 \rightarrow 1s2p\ ^3P_2$	3.3680	3.3678	⋯	⋯
He	$2s2p\ ^3P_2 \rightarrow 1s2s\ ^3S_1$	3.3718	3.3714	⋯	⋯
He	$2p^2\ ^3P_2 \rightarrow 1s2p\ ^3P_1$	3.3741	3.3733	⋯	⋯
He	$2s2p\ ^3P_1 \rightarrow 1s2s\ ^3S_1$	3.3756	3.3751	⋯	⋯
He	$2p^2\ ^3P_1 \rightarrow 1s2p\ ^3P_0$	3.3760	3.3752	⋯	⋯
He	$2p^2\ ^3P_1 \rightarrow 1s2p\ ^3P_1$	3.3767	3.3759	⋯	⋯
He	$2p^2\ ^3P_2 \rightarrow 1s2p\ ^3P_2$	3.3773	3.3765	⋯	⋯
He	$2s2p\ ^3P_0 \rightarrow 1s2s\ ^3S_1$	3.3771	3.3766	⋯	⋯
He	$2p^2\ ^3P_0 \rightarrow 1s2p\ ^3P_1$	3.3787	3.3779	⋯	⋯
He	$2p^2\ ^3P_1 \rightarrow 1s2p\ ^3P_2$	3.3799	3.3791	⋯	⋯
He-J	$2p^2\ ^1D_2 \rightarrow 1s2p\ ^1P_1$	3.3812	3.3806	⋯	⋯
He	$2p^2\ ^3P_2 \rightarrow 1s2p\ ^1P_1$	3.3905	3.3894	⋯	⋯
He	$2p^2\ ^3P_1 \rightarrow 1s2p\ ^1P_1$	3.3932	3.3919	⋯	⋯
He	$2p^2\ ^3P_0 \rightarrow 1s2p\ ^1P_1$	3.3951	3.3940	⋯	⋯
He	$2s2p\ ^3P_1 \rightarrow 1s2s\ ^1S_0$	3.3954	3.3953	⋯	⋯
He	$2s^2\ ^1S_0 \rightarrow 1s2p\ ^3P_1$	3.3996	3.3996	⋯	⋯
He	$2s^2\ ^1S_0 \rightarrow 1s2p\ ^1P_1$	3.4163	3.4159	⋯	⋯

dielectronic recombination satellite lines are the $2s2p\ ^1P_1 \rightarrow 1s2s\ ^1S_0$ line and the $2p^2\ ^1D_2 \rightarrow 1s2p\ ^1P_1$ line, which have been historically labeled as T and J, respectively. In particular, the ratio of T/Lyα_1 has been used to determine the electron temperature in previous works (see Bartiromo et al. 1985).

Because it may be difficult in observational or experimental measurements to resolve satellite T or even Lyα_1 from Lyα_2 we show in Figure 1(a) our calculations for the temperature dependence of $\Sigma I_{\rm DR}/I_{\rm Ly\alpha}$, which is the ratio of the flux from all dielectronic satellite lines in the range between 3.387 and 3.364 Å and the combined flux of both Lyα lines. These calculations were carried out with the SCRAM code. In Figure 1(a), we have plotted the electron temperature on the y-axis to stress that the temperature can be inferred from the measured $\Sigma I_{\rm DR}/I_{\rm Ly\alpha}$, ratio. The dependence is given for several different electron densities, ranging from 10^{10} to 10^{21} cm^{-3}, and essentially no such dependence is seen. The fact that the ratio of the sum of all dielectronic satellite lines to the sum of the two Lyα lines is sensitive to the electron temperature has also been pointed out by Gu (2012) in the case of the H-like Fe XXVI Lyα emission.

3. Experimental Results

The present experiments were carried out on the Orion laser facility (Hopps et al. 2015) with targets containing varying amounts of potassium. The data were collected with a recently developed high-resolution crystal spectrometer (Beiersdorfer et al. 2016) designed specifically for the determination of plasma characteristics from the line shape of X-ray lines produced by the Orion laser. The instrument is dubbed the Orion high-resolution X-ray (OHREX) spectrometer. In the present work, OHREX was fielded with a quartz $(10\bar{1}0)$ crystal (lattice spacing, 2d = 8.512 Å) that allowed for a wavelength

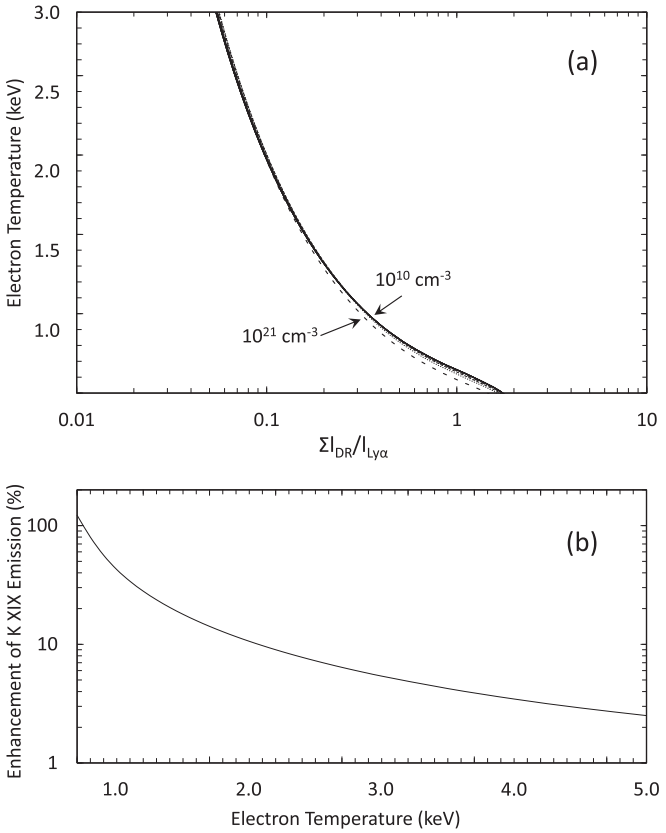

Figure 1. (a) Electron temperature vs. the ratio of $\Sigma I_{\rm DR}/I_{\rm Ly\alpha}$ for different electron densities and (b) percent enhancement of the K XIX emission feature vs. T_e due to the dielectronic satellite lines for the low-density limit ($n_e = 10^{10}$ cm^{-3}).

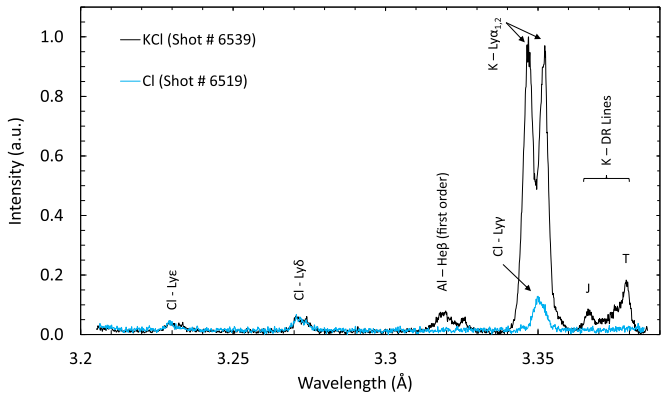

Figure 2. Time-integrated spectra from two OHREX measurements performed on the Orion laser employing a chlorinated plastic target and a KCl target. The wavelength scale shown is for second-order Bragg reflection. Aluminum features appear in first-order.

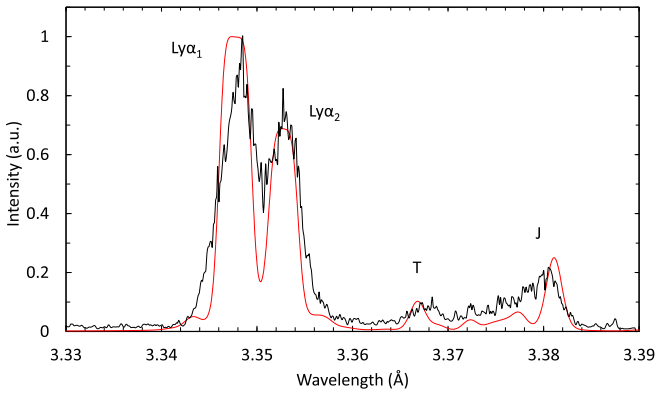

Figure 3. Measured and calculated spectra of H- and He-like emission of potassium. The OHREX measurement (black trace) was performed on the Orion laser employing a KF target (Orion shot #6523). The synthetic spectrum (smooth, red trace) was calculated with SCRAM using FAC data using $T_e = 1600$ eV and $n_e = 8 \times 10^{20}$ cm^{-3}.

coverage of 6.4–6.8 Å and a resolving power of approximately $E/\Delta E \approx 9000$. The present measurements were carried out in second-order Bragg reflection, i.e., 3.2–3.4 Å. Since OHREX employed an image plate for X-ray detection, all measurements were integrated over the entire shot.

The data of interest were collected with OHREX from six long-pulse Orion laser experiments, which irradiated thin foils (0.8–0.9 μm thick) typically with two 1.5 ns, 200 J pulses of 3ω light. The thin foils were of different compositions and are as follows: parylene dichloride (PyD; Orion shot # 6519), KF (Orion shot # 6523), KF/NaCl/KF (Orion shot # 6525), KF/KCl/KF (Orion shot # 6527), NaF/KCl/NaF (Orion shot # 6534), and KCl (Orion shot # 6539). The targets containing potassium were overcoated on one side with 0.025 μm Al and on both sides with 0.3 μm plastic. Aluminum line emission can be seen in first-order Bragg reflection unless a 8 μm thick Ti filter is used to screen out the first-order emission.

Two of our spectra are shown in Figure 2, one of the KCl target and the other of the PyD target. The chlorine spectrum includes the Lyγ $4p\,^2P_{3/2,1/2} \rightarrow 1s\,^2S_{1/2}$ lines, the Lyδ $5p\,^2P_{3/2,1/2} \rightarrow 1s\,^2S_{1/2}$ lines, and the Lyε $6p\,^2P_{3/2,1/2} \rightarrow 1s\,^2S_{1/2}$ lines, which were used to establish the dispersion in the wavelength calibration process. The wavelength values used for these chlorine lines come from Garcia & Mack (1965) and are 3.3508 Å, 3.2724 Å, and 3.2312 Å, respectively. In addition, the K Ly$\alpha_{1,2}$ $2p\,^2P_{3/2,1/2} \rightarrow 1s\,^2S_{1/2}$ lines at 3.3467 Å and 3.3521 Å, respectively, were used in the wavelength calibration process. Even with the dispersion known, and OHREX calibrated by Hell et al. (2016) for different crystals, each spectrum had to be uniquely calibrated, i.e., anchored to the Ly$\alpha_{1,2}$ lines, due to uncertainties in positioning the image plate in its holder and on the scanner. The resolution of OHREX can differentiate between the two K Ly$\alpha_{1,2}$ lines, with the Lyα_2 line blended with the Cl Lyγ line. In fact, the width of the lines shown in Figure 2 does not reflect the instrumental resolution; instead it is an expression of the opacity effects, plasma motion, and the ion temperature. It is also interesting to note that chlorine radiated approximately at the same relative intensities, whether it was in a mix with potassium or not.

The spectrum from the KF target (shot # 6523) is shown in Figure 3 along with the synthetic spectrum from our non-LTE potassium model from SCRAM. The SCRAM model includes opacity effects related to the finite thickness of the plasma, which is required to achieve a reasonable fit of relative intensities of the two Lyα lines. Although the fits we achieved between our modeling calculations and the measured spectrum are far from perfect, our modeling suggests an electron density on the order of 8×10^{20} cm^{-3}—although this density is only poorly constrained by the opacity affecting the relative intensity of the Lyα lines—and an electron temperature of approximately 1.6 keV. The standard error for our modeling has been previously reported as an order of magnitude for electron density and around 10% for electron temperature (Weller et al. 2014). In the present case, we double the uncertainty for the temperature because of the uncertainty in the intensity of the Lyα lines due to opacity effects.

The centroids of both T and J lines were estimated by Gaussian fitting for all five spectra and their wavelengths determined from our dispersion curve. The results are shown in Table 2. All experimental wavelength measurements have an error of approximately ± 0.0005 Å. The average measured value for T is 3.3668 Å and for J is 3.3792 Å, compared to the theoretical values of 3.3664 Å and 3.3812 Å, respectively, from FAC. The experimental value for J is found to be 0.0004 Å greater than that of FAC calculations, while that for T is 0.002 Å less.

4. Discussion and Conclusion

The K XIX $2p\,^2P_{3/2} \rightarrow 1s\,^2S_{1/2}$ Lyα_1 and Lyα_2 lines and the associated He-like dielectronic recombination satellite lines have been measured at electron temperatures near 1.6 keV. We showed that the ratio between the dielectronic satellite lines and the Lyα lines can be used to infer the electron temperature. In addition, the experimental wavelengths for the T and J dielectronic recombination lines were shown to be within 0.002 Å of calculations.

It would be useful to compare the measured ratio between the dielectronic satellite lines and the Lyα lines to spectral codes such as AtomDB (Foster et al. 2013) and SPEX (Kaastra et al. 1996). Although the K XIX Lyα lines are included in AtomDB, the He-like dielectronic lines to the K XIX Lyα spectrum are not. The reason for the omission may be that the K line positions in AtomDB derive from the NIST Atomic Spectra Database, which also only lists the Lyα lines but none of the satellite lines. Similarly, none of these dielectronic

Table 2
Experimental Wavelengths (Å) for the Two Strongest Potassium He-like Dielectronic Lines (Error for All Measurements is Approximately ±0.0005 Å)

Ion	Transition	Orion 6523	Orion 6525	Orion 6527	Orion 6534	Orion 6539	Average
He-T	$2s2p\ ^1P_1 \rightarrow 1s2s\ ^1S_0$	3.3670	3.3669	3.3669	3.3665	3.3668	3.3668
He-J	$2p^2\ ^1D_2 \rightarrow 1s2p\ ^1P_1$	3.3794	3.3793	3.3791	3.3791	3.3791	3.3792

satellite lines appear to be included in SPEX. Our present laboratory identification of these lines thus expands the list of "critically" evaluated atomic data for future use in these astrophysical plasma emission codes.

Bulbul et al. (2014) relied on AtomDB for calculating the flux of the K XIX lines. Because AtomDB does not include the associated He-like dielectronic satellite lines, it appears that their computed flux underestimates the contribution of the potassium line emission in their analysis of the 3.5 keV X-ray emission feature. The enhancement of the K XIX emission feature associated with the dielectronic satellite lines is given as a function of temperature in Figure 1(b). Although the enhancement at the temperature of maximum emission for the K XIX Lyα lines between 3 and 4 keV is only a few percent, it reaches up to 50% at 1 keV. Bulbul et al. (2019) have recently considered enhanced flux of the Ar XVII Heβ feature due to the dielectronic satellites, which may also affect the 3.5 keV feature. Their conclusion was that the added flux was not sufficient to account for the bulk of the 3.5 keV feature. This is also true for the added flux of the K XIX feature we studied here. However, each time additional flux is included in the plasma emission models the significance of the 3.5 keV feature diminishes, thus all such incremental enhancements must be accounted for.

The diagnostic importance of the Lyα spectra will certainly increase with future X-ray missions. The recent Hitomi spectrum of the Perseus cluster fell short of the expected observation length, and future missions will undoubtedly revisit this and other clusters with much higher spectral fidelity. Consequently, the statistical significance, thus the diagnostic utility of the K XIX spectrum and that of other H-like X-ray spectra will become very relevant for determining the electron temperatures associated with such ions.

This work was performed under the auspices of the U.S. DOE by LLNL under Contract No. DE-AC52-07NA27344. We thank Dr. Stephanie Hansen for making the SCRAM code available, as well as many helpful comments.

ORCID iDs

P. Beiersdorfer https://orcid.org/0000-0003-0127-599X

References

Aharonian, F. A., Akamatsu, H., Akimoto, F., et al. 2017, ApJL, 837, L15
Bartiromo, R., Bombarda, F., & Giannella, R. 1989, PhRvA, 40, 7387
Bartiromo, R., Giannella, R., Apicella, M. L., et al. 1985, Nucl. Instrum. Methods, 225, 378
Beiersdorfer, P., Bitter, M., van Goeler, S., & Hill, K. W. 1989, PhRvA, 40, 150
Beiersdorfer, P., Magee, E. W., Brown, G. V., et al. 2016, RScI, 87, 063501
Bulbul, E., Foster, A., Brown, G. V., et al. 2019, ApJ, 820, 21
Bulbul, E., Markevitch, M., Foster, A., et al. 2014, ApJ, 783, 13
Carlson, E., Jeltema, T., Profumo, S., et al. 2015, JCAP, 02, 009
Decaux, V., Bitter, M., Hsuan, H., et al. 1991, PhRvA, 43, 228
Feldman, U., Doschek, G. A., Nagel, D. J., Cowan, R. D., & Whitlock, R. R. 1974, ApJ, 192, 213
Foster, A. R., Ji, L., Yamaguchi, H., Smith, R. K., & Brickhouse, N. S. 2013, AIPCP, 1545, 252
Garcia, M. J., & Mack, J. E. 1965, JOSA, 55, 654
Gu, L., Kaastra, L., Raassen, A. J. J., et al. 2015, A&A, 584, L11
Gu, M. F. 2008, CaJPh, 86, 675
Gu, M. F. 2012, CaJPh, 90, 351
Hansen, S. B. 2011, CaJPh, 89, 633
Hansen, S. B., Bauche, J., Bauche-Arnoult, C., & Gu, M. F. 2007, HEDP, 3, 109
Hell, N., Beiersdorfer, P., Magee, E. W., & Brown, G. V. 2016, RSI, 87, 11D604
Hopps, N., Oades, K., Andrew, J., et al. 2015, PPCF, 57, 064002
Jeltema, T., & Profumo, S. 2015, MNRAS, 450, 2143
Johnson, W. R., & Soff, G. 1985, ADNDT, 33, 405
Kaastra, J. S., Mewe, R., & Nieuwenhuijzen, H. 1996, in 11th Coll. on UV and X-ray Spectroscopy of Astrophysical and Laboratory Plasmas, 411
Rice, J. E., Reinke, M. L., Ashbourn, J. M. A., et al. 2011, JPhB, 44, 165702
Rice, J. E., Reinke, M. L., Ashbourn, J. M. A., et al. 2014, JPhB, 47, 075701
Shah, C., Dobrodey, S., Bernitt, S., et al. 2016, ApJ, 833, 52
Vainshtein, L. A., & Safronova, U. I. 1978, ADNDT, 21, 49
Weller, M. E., Safronova, A. S., Kantsyrev, V. L., et al. 2014, PhPl, 21, 031206